JGR Solid Earth

RESEARCH ARTICLE
10.1029/2019JB018868

Key Points:
- A fast sweeping method is developed for computing the first-arrival traveltimes by solving the anisotropic eikonal equation in 2D TTI media
- The method is consistent and monotone

Supporting Information:
- Supporting Information S1

Correspondence to:
G. Huang,
HappyHuangSir@outlook.com

Citation:
Huang, G., Luo, S., Deng, J., & Vavryčuk, V. (2020). Traveltime calculations for qP, qSV, and qSH waves in two-dimensional tilted transversely isotropic media. *Journal of Geophysical Research: Solid Earth*, *125*, e2019JB018868. https://doi.org/10.1029/2019JB018868

Received 9 OCT 2019
Accepted 15 MAY 2020
Accepted article online 29 MAY 2020

Traveltime Calculations for qP, qSV, and qSH Waves in Two-Dimensional Tilted Transversely Isotropic Media

Guangnan Huang[1,2], Songting Luo[2], Juzhi Deng[1], and Václav Vavryčuk[3]

[1]Department of Geophysics, East China University of Technology, Nanchang, China, [2]Department of Mathematics, Iowa State University, Ames, IA, USA, [3]Institute of Geophysics, The Czech Academy of Science, Praha, Czech Republic

Abstract This paper presents a fast sweeping method (FSM) to calculate the first-arrival traveltimes of the qP, qSV, and qSH waves in two-dimensional (2D) transversely isotropic media, whose symmetry axis may have an arbitrary orientation (tilted transverse isotropy [TTI]). The method discretizes the anisotropic eikonal equation with finite difference approximations on a rectangular mesh and solves the discretized system iteratively with the Gauss-Seidel iterations along alternating sweeping orderings. At each mesh point, a highly nonlinear equation is solved to update the numerical solution until its convergence. For solving the nonlinear equation, an interval that contains the solutions is first determined and partitioned into few subintervals such that each subinterval contains one solution; then, the false position method is applied on these subintervals to compute the solutions; after that, among all possible solutions for the discretized equation, a causality condition is imposed, and the minimum solution satisfying the causality condition is chosen to update the solution. For problems with a point-source condition, the FSM is extended for solving the anisotropic eikonal equation after a factorization technique is applied to resolve the source singularities, which yields clean first-order accuracy. When dealing with the triplication of the qSV wave, solutions corresponding to the minimal group velocity are chosen such that continuous solutions are computed. The accuracy, efficiency, and capability of the proposed method are demonstrated with numerical experiments.

1. Introduction

The traveltimes of seismic waves are often used to study the interior structure of the Earth. Numerical methods for calculating the traveltimes of seismic waves play an important role in many seismic techniques, such as raypath backtracking, quality factor inversion, formation stress inversion, and Kirchhoff prestack depth migration. Accurate traveltimes can be calculated by ray-tracing methods and finite difference eikonal solvers. The ray-tracing method computes the traveltimes by solving an appropriate initial or boundary value problem for a system of ordinary differential equations. It can provide high-order accuracy for the traveltime tables (Cerveny, 1972; Shearer & Chapman, 1988). However, (1) raypaths often diverge from each other, and large spatial gaps often exist between two adjacent rays, especially in complicated heterogeneous velocity models (Vidale, 1990); (2) traveltimes are only calculated for shot-receiver pairs such that they must be interpolated onto a large number of grid nodes when they are used for seismic migration and tomography (Gray & May, 1994; Huang & Bellefleur, 2012; Vinje et al., 1993); (3) the two-point ray-tracing problem can be highly nonlinear such that it is difficult to solve efficiently; and (4) it can be difficult or time-consuming to distinguish whether the solution is a first or later arrival where triplication occurs. On the contrary, the eikonal solvers such as the finite difference traveltime calculation methods have no such disadvantages. For the past four decades, many eikonal solvers have been developed (Cao & Greenhalgh, 1993; Fomel et al., 2009; Hole & Zelt, 1995; Kim, 2002; Lan et al., 2014; Podvin & Lecomte, 1991; Sethian & Popovici, 1999; Stovas & Alkhalifah, 2012; Vidale, 1988; Zhao, 2005). Among these eikonal solvers, the fast marching method (FMM) and the fast sweeping method (FSM) are the two most popular ones. It is worth noting that finite difference eikonal solvers in general can only compute first arrivals. They may require well-designed numerical procedures for solving a complicated nonlinear system, and the number of iterations are problem dependent if an iterative scheme is used.

The kinematic and dynamic features of seismic waves have great differences when they propagate in isotropic and anisotropic media. In isotropic media, only compressional and shear waves exist. While in anisotropic media, there may have three wave modes: one quasi-compressional wave (qP) and two quasi-shear waves (qS1 and qS2). Each wave mode propagates with its own wave speed and polarization. The phase and group velocities of each wave mode are not only functions of elastic moduli parameters but also functions of the propagation direction. Many finite difference eikonal solvers have already been extended to calculate the traveltimes of seismic waves in anisotropic media (Dellinger & Symes, 1997; Eaton, 1993; Kim & Cook, 1999; Lecomte, 1993; Perez & Bancroft, 2001; Qian & Symes, 2002a). But most of them have been developed to deal with the tilted elliptically anisotropic (TEA) case only, for example, the fast marching method for the TEA eikonal equation (Cristiani, 2009; Lou, 2006; Sethian & Vladimirsky, 2003) and the FSM for the TEA eikonal equation (Luo & Qian, 2012; Qian et al., 2007; Tsai et al., 2003). Han et al. (2017) developed an FSM, which uses a quartic solver to tackle the quartic equation of the slowness surface with limited value range for the possible solutions, and obtained the traveltime of the qP wave. Bouteiller et al. (2018) developed a time-dependent discontinuous Galerkin method for computing the traveltime of the qP wave in 2D cases by transferring the static quartic anisotropic eikonal equation into a time-dependent equation. Waheed et al. (2015) and Waheed and Alkhalifah (2017) proposed an iterative FSM, like the fixed-point iteration method, to compute the traveltime of the qP wave by solving a sequence of TEA eikonal equations, where the slowness field of the TEA eikonal equation is updated iteratively whenever the numerical solution is updated until it converges to the solution of the original quartic anisotropic eikonal equation.

Finite difference eikonal solvers are efficient. However, they all suffer from the source singularities due to the nondifferentiability of the solution at the point source (Qian & Symes, 2002b). The source singularities induce large errors near the source, which will further spread to the whole computational domain and make the traveltime inaccurate. Without any treatments of the source singularities, such methods, even high-order methods, have only $O(h\log h)$ convergence order with the mesh size h. Moreover, this poses a problem to calculate some quantities involving derivatives of the traveltime, such as take-off angles and geometric spreading factors (Noble et al., 2014). This also poses a problem for iterative eikonal solvers involving derivatives of the traveltime as in Waheed et al. (2015). In order to overcome the difficulty caused by the source singularities, several different methods have been proposed. The first method wraps a small region around the source, assumes that the medium in the region is homogeneous such that the analytical solution can be obtained, and carries out the computation only outside of this region (Sethian & Popovici, 1999). This method is feasible only when the medium around the source is homogeneous. The second method refines the grid around the source in order to compensate the truncation error, but it involves ad hoc parameters without a clear selection criterion (Kim & Cook, 1999; Rawlinson et al., 2008). The third method uses an adaptive grid refinement near the source to control the error, but it incurs an additional heavy computational burden (Qian & Symes, 2002b). And the fourth method makes finite difference approximations for the eikonal equation on spherical grids centered on the source point in order to reduce inaccuracy (Alkhalifah & Fomel, 2001). However, the final result has to be interpolated to traveltime tables in Cartesian coordinates, which increases the computational cost.

In order to resolve the source singularities effectively without involving ad hoc parameters, a factorization approach has been proposed in Pica (1997), Zhang et al. (2005), Fomel et al. (2009), Luo and Qian (2012), and Waheed and Alkhalifah (2017) for the isotropic eikonal equation and anisotropic eikonal equation with weak anisotropy. The traveltime is factored into two factors. One factor is a known function that captures the singularities around the source, and the other factor is smooth near the source. The smooth factor satisfies a modified/factored equation that can be solved efficiently with high accuracy. Hence, the original traveltime is recovered with high accuracy. Luo and Qian (2011) and Luo et al. (2012) extended this factorization method to higher-order schemes to calculate first-arrival traveltimes and amplitudes. Treister and Haber (2016) and Treister and Haber (2017) used the first-order and second-order finite difference schemes in the fast marching method to solve the factored eikonal equation. Luo and Qian (2012) gave a systematic procedure to obtain analytical approximations for the known factor that captures the source singularities and extended the factorization approach to eikonal equation in the TEA media. Following this approach, Tavakoli et al. (2015), Waheed and Alkhalifah (2017) and Waheed et al. (2014) proposed an iterative factored eikonal solver for computing the first-arrival traveltime of the qP wave in TTI media with a simplified formulation of the anisotropic eikonal equation. Bouteiller et al. (2018) extended the factorization approach to a high-order method in the framework of discontinuous

Galerkin method by transforming the simplified anisotropic eikonal equation into a time-dependent equation.

In review of the traveltime calculation methods in anisotropic media with the finite difference schemes, one finds that most of them are the eikonal solvers for the qP wave governed by a weak or simplified anisotropic eikonal equation, because the qSV wave involves a triplication phenomenon when several qSV waves can propagate along the same raypath (Vavrycuk, 2003a, 2006). This phenomenon is mostly associated with strong anisotropy or with directions close to point singularities in anisotropy (Vavrycuk, 2003b). In this work, we propose an anisotropic eikonal solver for the qP, qSV, and qSH waves, in the framework of the FSM, in 2D TTI media with arbitrary anisotropic strength. The method has the following important features: (1) the anisotropic eikonal equation is discretized on a mesh covering the computational domain; (2) the coupled system of the discretized equations among all grid points is solved iteratively by combining the Gauss-Seidel iterations with alternating sweeping orderings; (3) at each grid point, the subintervals that contain the solutions of the discretized equation are predetermined such that each subinterval contains exactly one solution at most, and the false position method can be applied to compute the solutions efficiently; (4) among all possible solutions at a grid point, a causality condition is imposed to pick the one that corresponds to the first-arrival traveltime; (5) the scheme is monotone, and the numerical solution will converge to the viscosity solution as the mesh size approaches 0; and (6) the medium can have arbitrary anisotropic strength, and the symmetric axis of the anisotropic medium can have arbitrary orientation. These features make the eikonal solver more applicable to general situations and can obtain first-arrival traveltimes for the three waves. In order to resolve the source singularities for the anisotropic eikonal equation with point-source conditions, the factorization approach is applied such that a factored anisotropic eikonal equation is derived. The proposed anisotropic eikonal solver is further extended to solve the factored anisotropic eikonal equation following the similar procedures, which results in the FSMs for the factored anisotropic eikonal equation. The proposed methods enjoy all the appealing features of the usual FSM. The number of iterations are independent of the mesh size, and the numerical solution will converge to the desired weak solution as the mesh size approaches 0.

The paper is organized as follows: the general anisotropic eikonal equation for TTI media and the factored anisotropic eikonal equations by use of the multiplicative and additive factorization techniques are introduced in section 2. The numerical schemes in the framework of the FSM for solving the general and factored anisotropic eikonal equations are presented in section 3. Several anisotropic models are used in the numerical experiments to verify the accuracy and efficiency of the proposed methods, which are discussed in section 4. Conclusive remarks are given at the end.

2. Anisotropic Eikonal Equation

The determination of the traveltimes of seismic waves in general anisotropic media involves solving a sixth-order partial differential equation, that is, the Christoffel equation (Cerveny, 2001),

$$det\left|a_{ijkl}n_jn_l - v^2\delta_{ik}\right| = 0, \tag{1}$$

where a_{ijkl} is a rank-4 density normalized stiffness tensor, $\mathbf{n}$ is the normal vector of the wavefront, v is the phase velocity, and δ_{ik} is the Kronecker delta function. From the Christoffel equation and by introducing the slowness vector $\mathbf{p} = \frac{\mathbf{n}}{v}$, one can derive the anisotropic eikonal equation as

$$v|\nabla T| = 1, \tag{2}$$

where T is the traveltime and $\mathbf{p} = \nabla T$. In 2D cases, Equation 2 can be rewritten as

$$H(P,\ Q) \equiv v_m\sqrt{P^2 + Q^2} - 1 = 0,\ \ (m = 1,\ 2,\ 3), \tag{3}$$

where $v_m (m = 1,2,3)$ is the phase velocity for the qP, qSV, and qSH waves, respectively, and $(P,Q) = (T_x,T_y)$. A general 2D TTI medium can be defined by five elastic moduli $\{a_{11},a_{13},a_{33},a_{44},a_{66}\}$ and the angle of the symmetry axis θ_0 (Thomsen, 1986). The expressions for v_m corresponding to the three wave modes are given as (Daley & Hron, 1977; Zhou & Greenhalgh, 2004)

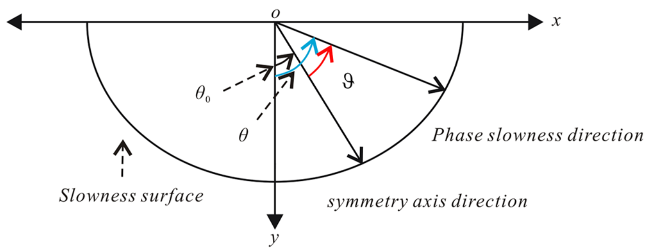

Figure 1. Definition of three different angles: (a) ϑ is the angle between the phase slowness direction and the symmetry axis direction. (b) θ is the angle between the phase slowness direction and the vertical y-axis. (c) θ_0 is the angle between the symmetry axis direction and the vertical y-axis.

$$\begin{aligned} v_{1,2} &= \sqrt{M \pm \sqrt{M^2 - N}}, \\ v_3 &= \sqrt{a_{44} + (a_{66} - a_{44})\sin^2\vartheta}, \end{aligned} \tag{4}$$

where M and N are defined as

$$\begin{aligned} M &= 0.5(K_1 + K_2), \\ N &= K_1 K_2 - K_3, \end{aligned} \tag{5}$$

and

$$\begin{aligned} K_1 &= a_{44}\cos^2\vartheta + a_{11}\sin^2\vartheta, \\ K_2 &= a_{33}\cos^2\vartheta + a_{44}\sin^2\vartheta, \\ K_3 &= 0.25(a_{13}+a_{44})^2\sin^2 2\vartheta. \end{aligned} \tag{6}$$

Here the angle ϑ is formed by the phase slowness direction and the direction of the symmetry axis of the medium, that is, $\vartheta = \theta - \theta_0$ with θ as the phase slowness angle. The relationship of these three angles is illustrated in Figure 1. According to Thomsen (1986), the phase slowness angle θ is formed by the wavefront normal and the vertical axis of the medium, and it can be computed by

$$\theta = \arccos\left(\frac{Q}{\sqrt{P^2 + Q^2}}\right). \tag{7}$$

With Equations 4 to 7, the phase velocity v_m can be computed for an anisotropic TTI media, and v_m depends on the phase slowness angle θ.

2.1. Multiplicatively Factored Anisotropic Eikonal Equation

The multiplicative factorization method decomposes the solution of Equation 2 as a product of two factors: the first factor is calculated analytically or numerically to capture the source singularities, and the second factor is a smooth correction near the source. Let us consider a multiplicatively factored decomposition,

$$T = T_0 \tau, \tag{8}$$

where T_0 is the predetermined factor to capture the source singularities and τ is the unknown factor that is smooth near the source.

Substituting Equation 8 into Equation 2 yields the following multiplicatively factored anisotropic eikonal equation for τ,

$$v_m |(P_1,\ Q_1)| = 1, \quad (m = 1,\ 2,\ 3), \tag{9}$$

with P_1 and Q_1 defined as

$$\begin{aligned} P_1 &= T_{0x}\tau + T_0\tau_x, \\ Q_1 &= T_{0y}\tau + T_0\tau_y. \end{aligned} \tag{10}$$

Then, Equation 9 can be rewritten as

$$H(P_1,\ Q_1) \equiv v_m\sqrt{P_1^2 + Q_1^2} - 1 = 0, \quad (m = 1,\ 2,\ 3). \tag{11}$$

2.2. Additively Factored Anisotropic Eikonal Equation

For the additively factored method, the traveltime T is decomposed as

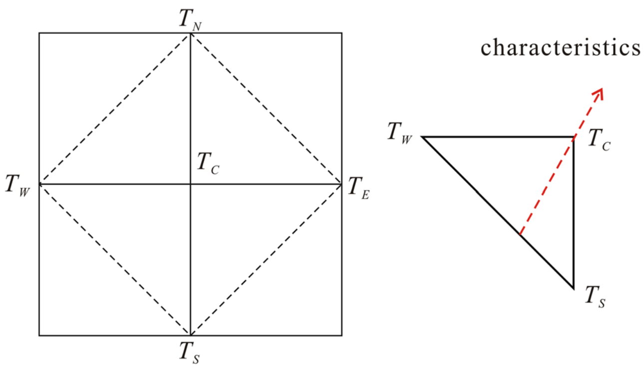

Figure 2. Rectangular mesh in the 2D case. Four triangles (ΔCEN, ΔCNW, ΔCWS, and ΔCSE) are used to calculate traveltime candidates for the center grid point C.

$$T = T_0 + \tau, \tag{12}$$

where T_0 and τ are defined similarly.

Substituting Equation 12 into Equation 2 yields the additively factored anisotropic eikonal equation for τ,

$$v_m |(P_2,\ Q_2)| = 1,\ \ (m = 1,\ 2,\ 3), \tag{13}$$

with P_2 and Q_2 defined as

$$\begin{aligned} P_2 &= T_{0x} + \tau_x, \\ Q_2 &= T_{0y} + \tau_y. \end{aligned} \tag{14}$$

Then, Equation 13 can be rewritten as

$$H(P_2,\ Q_2) \equiv v_m \sqrt{P_2^2 + Q_2^2} - 1 = 0,\ \ (m = 1,\ 2,\ 3). \tag{15}$$

3. Fast Sweeping Method

To compute the first-arrival traveltimes for the three wave modes, we will solve the anisotropic eikonal Equation 3 numerically in the sense of viscosity solutions, for which the FSM is presented. For simplicity, we illustrate the scheme on a uniform mesh ($n_x \times n_y$) covering the rectangular computational domain, with mesh size (h_x,h_y). We take $h_x = h_y = h$ for notational simplicity.

3.1. General Eikonal Equation

Figure 2 shows an interior grid point C with four neighboring grid points W, E, N, and S. The anisotropic eikonal equation can be discretized on the four triangles associated with point C: ΔCEN, ΔCNW, ΔCWS, and ΔCSE. Taking ΔCWS as an example, the discretized eikonal equation can be written as

$$v_m \left| \left(\frac{T_C - T_W}{h},\ \frac{T_C - T_S}{h} \right) \right| - 1 = 0,\ \ (m = 1,\ 2,\ 3), \tag{16}$$

where T_W and T_S are traveltimes at grid points W and S, respectively.

Given T_W and T_S, Equation 16 must be solved to find solutions for T_C at C. Similarly, the anisotropic eikonal Equation 3 is discretized on the remaining three triangles and is solved for solutions T_C at C with given neighbor values. For each possible solution for T_C, it is required to satisfy a causality condition such that it becomes a candidate for updating T_C at C. The causality condition is related to the characteristic direction,

$$\begin{aligned} \frac{\partial H}{\partial P} &= \frac{P}{\sqrt{P^2 + Q^2}} v_m(\theta) - \frac{Q}{\sqrt{P^2 + Q^2}} \frac{\partial v_m}{\partial \theta}, \\ \frac{\partial H}{\partial Q} &= \frac{Q}{\sqrt{P^2 + Q^2}} v_m(\theta) + \frac{P}{\sqrt{P^2 + Q^2}} \frac{\partial v_m}{\partial \theta}. \end{aligned} \tag{17}$$

In triangle ΔCWS, it requires $\frac{\partial H}{\partial P} \geq 0$ and $\frac{\partial H}{\partial Q} \geq 0$. In general, the causality condition requires that (H_P,H_Q) passes through C and lies in the triangle used in the discretization. Then, for all possible candidates for T_C from all the four triangles, we pick the minimum one that corresponds to the first-arrival traveltime. If there are no candidates, T_C will be updated along the edges, for example, on triangle ΔCWS,

$$T_C = \min\left(T_W + \frac{h}{U_m^{WC}},\ T_C + \frac{h}{U_m^{SC}} \right),\ \ (m = 1,\ 2,\ 3), \tag{18}$$

where U_m^{WC} and U_m^{SC} are group velocities along edges $\overrightarrow{WC}$ and $\overrightarrow{SC}$, respectively.

The discretized Equation 16 at all grid points is coupled together to form a system of nonlinear equations that can be solved using the Gauss-Seidel iteration with alternating sweeping orderings, which is the FSM.

Algorithm Sketch: FSM for Anisotropic Eikonal Equation

1. Initialization: assigning exact/approximate values at grid points according to given boundary conditions, which will be fixed during the iterations, and assigning large positive values at all other grid points.
2. Gauss-Seidel iteration: sweeping the computational domain with four alternating orderings iteratively:

$$
\begin{aligned}
&(a)\ i = 1{:}n_x,\ j = 1{:}n_y, \qquad &&(b)\ i = 1{:}n_x,\ j = n_y{:}1,\\
&(c)\ i = n_x{:}1,\ j = 1{:}n_y, \qquad &&(d)\ i = n_x{:}1,\ j = n_y{:}1,
\end{aligned}
$$

and at each grid point C, updating T_C according to the above numerical procedure.

3. Termination: terminating the iteration if the L_1-norm difference of the solutions between two successive iterations is smaller than the specified accuracy requirement.

During the Gauss-Seidel iteration of the FSM, the discretized Equation 16 must be solved efficiently, and the group velocity along edges needs to be computed.

3.2. Multiplicatively Factored Eikonal Equation

Taking ΔCWS as an example, the discretized equation of the multiplicatively factored eikonal equation can be written as

$$v_m|(P_1,\ Q_1)| - 1 = 0,\ \ (m = 1,\ 2,\ 3), \tag{19}$$

where P_1 and Q_1 are defined as

$$
\begin{aligned}
P_1 &= T_{0x}\tau_C + T_0\frac{\tau_C - \tau_W}{h},\\
Q_1 &= T_{0y}\tau_C + T_0\frac{\tau_C - \tau_S}{h}.
\end{aligned} \tag{20}
$$

Given τ_W and τ_S, this equation can be solved to find solutions for τ_C at C. Similarly, each possible solution for τ_C should satisfy a causality condition such that it becomes a candidate for updating τ_C at C. The causality condition is similar as above with the characteristic direction given by

$$
\begin{aligned}
\frac{\partial H}{\partial P_1} &= \frac{P_1}{\sqrt{P_1^2 + Q_1^2}}v_m(\theta) - \frac{Q_1}{\sqrt{P_1^2 + Q_1^2}}\frac{\partial v_m}{\partial \theta},\\
\frac{\partial H}{\partial Q_1} &= \frac{Q_1}{\sqrt{P_1^2 + Q_1^2}}v_m(\theta) + \frac{P_1}{\sqrt{P_1^2 + Q_1^2}}\frac{\partial v_m}{\partial \theta}.
\end{aligned} \tag{21}
$$

In triangle ΔCWS, it requires $\frac{\partial H}{\partial P_1} \ge 0$ and $\frac{\partial H}{\partial Q_1} \ge 0$. Similarly, the factored anisotropic eikonal equation must be discretized and solved on the remaining three triangles. And from all possible candidates for τ_C that satisfy the causality condition, we pick the minimum one corresponding to the first-arrival traveltime. If there are no candidates, we will update τ_C along the edges in the following way as in Fomel et al. (2009) and Luo and Qian (2012).

The characteristic equations of the multiplicatively factored eikonal equation are given as

$$
\begin{aligned}
\left(\frac{dx}{dt}, \frac{dy}{dt}\right) &= \left(\frac{\partial H}{\partial p}, \frac{\partial H}{\partial q}\right) = T_0\left(\frac{\partial H}{\partial P_1}, \frac{\partial H}{\partial Q_1}\right),\\
\frac{d\tau}{dt} &= (p,\ q)\left(\frac{\partial H}{\partial p}, \frac{\partial H}{\partial q}\right)^T = 1 - \left(T_{0x}\frac{\partial H}{\partial P_1} + T_{0y}\frac{\partial H}{\partial Q_1}\right)\tau,
\end{aligned} \tag{22}
$$

where $(p,q) = (\tau_x, \tau_y)$ are derivatives of τ with respect to x and y, respectively. According to the first equation, we have

$$\left(\frac{dx}{dt}\right)^2 + \left(\frac{dy}{dt}\right)^2 = T_0^2 U_m^2, \quad (m = 1,\ 2,\ 3), \tag{23}$$

where U_m is the group velocity that will be defined in Equation 34. Using the method of characteristics, we can approximate τ_C at C along the edge $\overrightarrow{WC}$ (or $\overrightarrow{SC}$) by imposing that the ray falls on $\overrightarrow{WC}$ (or $\overrightarrow{SC}$). Let us take the edge $\overrightarrow{WC} = (\delta x, \delta y)$ as an example. According to Equation 23, we have

$$\delta t = \frac{\sqrt{\delta x^2 + \delta y^2}}{T_0 U_m}, \quad (m = 1,\ 2,\ 3). \tag{24}$$

Then, from the second equation of the characteristic equations, the approximation for τ_C, denoted as τ_{WC}, can be computed by

$$\tau_{WC} = \frac{\tau_W + \delta t}{1 + T_{0x}\frac{\delta x}{T_0} + T_{0y}\frac{\delta y}{T_0}}. \tag{25}$$

Similarly, τ_C can also be calculated along $\overrightarrow{SC}$, denoted as τ_{SC}. And we will pick the minimal one by min $\{\tau_{WC},\ \tau_{SC}\}$ to update τ_C at C.

The discretized Equation 19 at all grid points is coupled together to form a system of nonlinear equations. This set of nonlinear equations can be solved similarly using the FSM. The algorithmic sketch of the FSM for the multiplicatively factored eikonal equation is similar to that of the general eikonal equation. However, the latter one involves three extra parameters T_0, T_{0x}, and T_{0y}.

3.3. Additively Factored Eikonal Equation

Similarly, taking ΔCWS as an example, the discretized equation of the additively factored eikonal equation can be written as

$$v_m |(P_2,\ Q_2)| - 1 = 0, \quad (m = 1,\ 2,\ 3), \tag{26}$$

where P_2 and Q_2 are defined as

$$P_2 = T_{0x} + \frac{\tau_C - \tau_W}{h},\ Q_2 = T_{0y} + \frac{\tau_C - \tau_S}{h}. \tag{27}$$

Given τ_W and τ_S, this equation can also be solved to find solutions for τ_C at C. A similar causality condition is imposed on the solution such that it becomes a candidate for updating τ_C at C. The characteristic direction for the additively factored eikonal equation is given as

$$\begin{aligned} \frac{\partial H}{\partial P_2} &= \frac{P_2}{\sqrt{P_2^2 + Q_2^2}} v_m(\theta) - \frac{Q_2}{\sqrt{P_2^2 + Q_2^2}} \frac{\partial v_m}{\partial \theta}, \\ \frac{\partial H}{\partial Q_2} &= \frac{Q_2}{\sqrt{P_2^2 + Q_2^2}} v_m(\theta) + \frac{P_2}{\sqrt{P_2^2 + Q_2^2}} \frac{\partial v_m}{\partial \theta}. \end{aligned} \tag{28}$$

In triangle ΔCWS, it requires $\frac{\partial H}{\partial P_2} \geq 0$ and $\frac{\partial H}{\partial Q_2} \geq 0$. Similarly, from all possible candidates that satisfy the causality condition, the minimum one is chosen to update τ_C at C. If there are no candidates, τ_C will be calculated along the two edges $\overrightarrow{WC}$ and $\overrightarrow{SC}$, respectively.

The characteristic equations of the additively factored eikonal equation are given as

$$
\begin{aligned}
\left(\frac{dx}{dt}, \frac{dy}{dt}\right) &= \left(\frac{\partial H}{\partial p}, \frac{\partial H}{\partial q}\right) &&= \left(\frac{\partial H}{\partial P_2}, \frac{\partial H}{\partial Q_2}\right), \\
\frac{d\tau}{dt} &= (p,\ q)\left(\frac{\partial H}{\partial p}, \frac{\partial H}{\partial q}\right)^T &&= 1 - \left(T_{0x}\frac{\partial H}{\partial P_2} + T_{0y}\frac{\partial H}{\partial Q_2}\right).
\end{aligned} \tag{29}
$$

According to the first equation, we have

$$\left(\frac{dx}{dt}\right)^2 + \left(\frac{dy}{dt}\right)^2 = U_m^2,\ \ (m = 1,\ 2,\ 3). \tag{30}$$

Using the method of characteristics, we can compute τ_C at C along the edge $\overrightarrow{WC}$ (or $\overrightarrow{SC}$) by imposing that the ray falls on $\overrightarrow{WC}$ (or $\overrightarrow{SC}$). Let us take the edge $\overrightarrow{WC} = (\delta x, \delta y)$ as an example. According to Equation 30, we have

$$\delta t = \frac{\sqrt{\delta x^2 + \delta y^2}}{U_m},\ \ (m = 1,\ 2,\ 3). \tag{31}$$

According to the second equation of the characteristic equations, the approximation for τ_C, denoted as τ_{WC}, can be computed as

$$\tau_{WC} = \tau_W + \delta t - \left(T_{0x}\delta x + T_{0y}\delta y\right). \tag{32}$$

Similarly, τ_C can also be calculated along $\overrightarrow{SC}$, denoted as τ_{SC}. And the minimum one, $\min\{\tau_{WC},\ \tau_{SC}\}$, is chosen to update τ_C at C.

The algorithmic sketch of the FSM for the additively factored eikonal equation is also similar to that of the general eikonal equation. And it also involves three extra parameters T_0, T_{0x}, and T_{0y}.

3.4. Calculation of Traveltime T_0

For the two factorization techniques, T_0 should be computed for a homogeneous anisotropic model, where the medium parameters are assigned as those of the orginal model at the source point. T_0 can be computed as

$$T_0^m(\mathbf{x}) = \frac{|\mathbf{x} - \mathbf{x_0}|}{U_m(\theta)},\ \ (m = 1,\ 2,\ 3), \tag{33}$$

where $\mathbf{x_0}$ is the source position and $\mathbf{x}$ is a position in the model domain. $U_m(\theta)$ is the group velocity along the ray direction $\mathbf{x}-\mathbf{x_0}$.

The expression of the group velocity can be found in previous work (Berryman, 1979),

$$U_m^2 = v_m^2 + \left(\frac{\partial v_m}{\partial \vartheta}\right)^2,\ \ (m = 1,\ 2,\ 3), \tag{34}$$

where

$$
\begin{aligned}
\frac{\partial v_{1,2}}{\partial \vartheta} &= \frac{1}{2v_{1,2}}\left[\frac{\partial M}{\partial \vartheta} \pm \frac{M\frac{\partial M}{\partial \vartheta} - 0.5\frac{\partial N}{\partial \vartheta}}{\sqrt{M^2 - N}}\right], \\
\frac{\partial v_3}{\partial \vartheta} &= \frac{(a_{66} - a_{44})}{2v_3}\sin 2\vartheta,
\end{aligned} \tag{35}
$$

and

$$
\begin{aligned}
\frac{\partial M}{\partial \vartheta} &= 0.5(a_{11} - a_{33})\sin 2\vartheta, \\
\frac{\partial N}{\partial \vartheta} &= [K_1(a_{44} - a_{33}) + K_2(a_{11} - a_{44})]\sin 2\vartheta - 0.5(a_{44} + a_{13})^2 \sin 4\vartheta.
\end{aligned} \tag{36}
$$

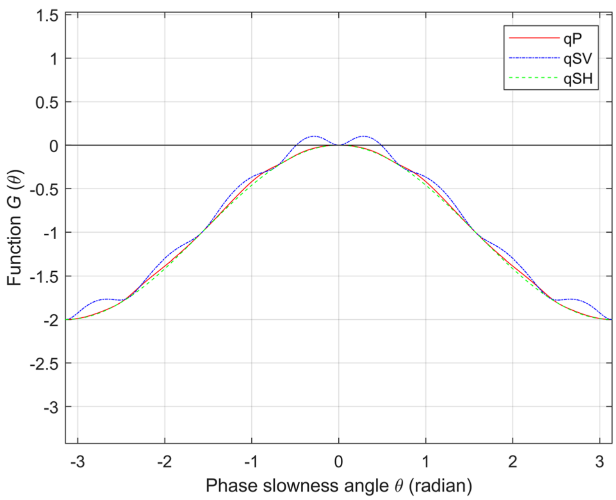

Figure 3. Function $G(\theta)$ for three wave modes (qP, qSV, and qSH waves) in the homogeneous anisotropic model with the inclination angle $\theta_0 = 0^o$.

The phase slowness angle θ, as well as the angle ϑ, is defined implicitly in that they depend on the solution T. We will present a numerical procedure to compute the group velocity and phase velocity along a ray direction in section 3.8.

3.5. Solving the Discretized Equation 16

At grid point C, the discretized Equation 16 must be solved among all the four triangles. The equation is highly nonlinear in T_C, and it may have multiple solutions for T_C. Therefore, solving Equation 16 for T_C is challenging. We present our numerical procedures for solving the equation: (1) determine an interval that contains all possible solutions, (2) partition the interval into subintervals such that each subinterval contains exactly one solution, and (3) apply false position method to find the solution in each subinterval (Press et al., 1992). We elaborate the numerical procedures by taking ΔCWS as an example.

According to the Fermat's principle, the interval that contains all possible values for T_C is

$$I_{WS} \equiv \left[\min(T_W,\ T_S),\ \min\left(T_W + \frac{h}{U_m^{WC}},\ T_S + \frac{h}{U_m^{SC}}\right)\right],\quad (m = 1,\ 2,\ 3). \tag{37}$$

In order to determine subintervals that contain exactly one solution, we need to locate the extrema of H as a function of T_C and use the extreme points to partition the interval into few subintervals (see Figure 6). We can determine the extreme points by calculating the critical points through

$$\frac{\partial H}{\partial T_C} = \frac{\partial H}{\partial P}\frac{\partial P}{\partial T_C} + \frac{\partial H}{\partial Q}\frac{\partial Q}{\partial T_C} = 0, \tag{38}$$

which is an equation of the angle θ after algebraic manipulation, that is,

$$F(\theta) \equiv \left(\sin\theta v_m(\theta) - \cos\theta\frac{\partial v_m}{\partial\theta} + \cos\theta v_m(\theta) + \sin\theta\frac{\partial v_m}{\partial\theta}\right)\frac{1}{h} = 0. \tag{39}$$

Therefore, we can solve Equation 39 for all possible solutions θ_i and then find corresponding extreme points for H as a function of T_C through

$$T_C^i = \frac{\sin\theta_i T_S - \cos\theta_i T_W}{\sin\theta_i - \cos\theta_i},\quad (i = 1,\ 2,\ 3,\ \ldots\ ). \tag{40}$$

We note that the solutions for $F(\theta)$ can be precomputed and saved. Then, during the Gauss-Seidel iteration, T_C^i are computed through formula (40) to partition the interval I_{WS} into subintervals. Once the subintervals are determined, we can simply apply the false position method to find the solution in each subinterval; hence, we can find all solutions in the interval I_{WS}.

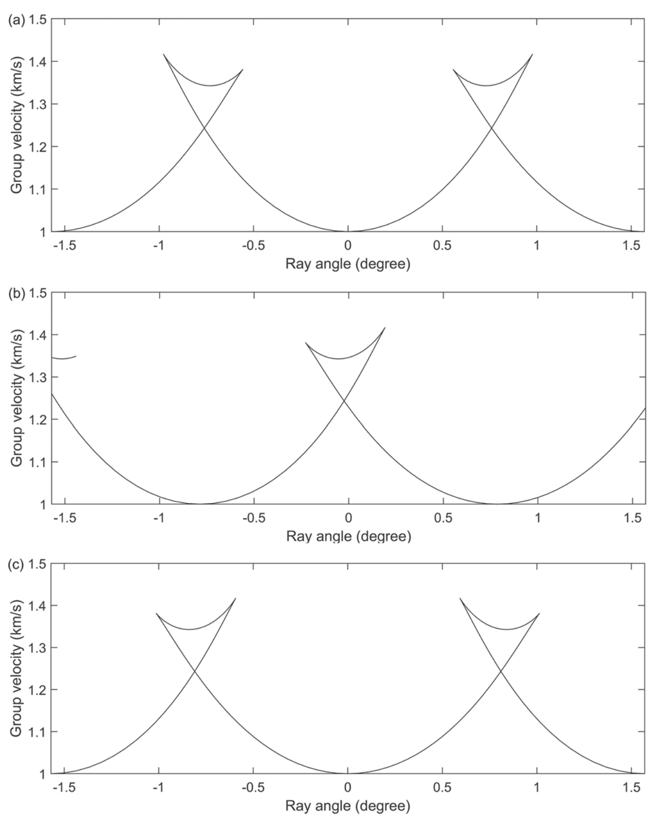

Figure 4. Group velocities of the qSV wave mode for three different directions of the symmetry axis ($\theta_0 = 0°$, 45°, and 90°). The group velocity is plotted against the ray angle from $-\pi/2$ to $\pi/2$.

3.6. Solving the Discretized Equation 19

Similarly, at grid point C, the discretized Equation 19 needs to be solved in all the four triangles. The equation is also highly nonlinear in τ_C, and it may have multiple solutions for τ_C. In order to introduce the procedures conveniently, we also take ΔCWS as an example.

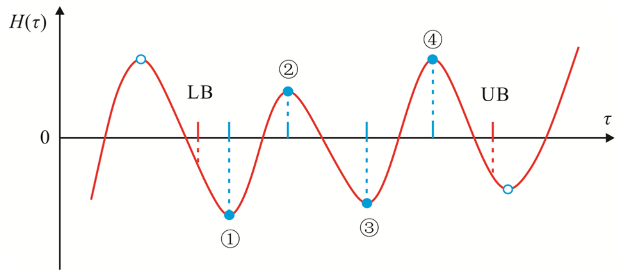

Figure 5. Extreme points of the eikonal equation partition the solution interval I_{WS} into subintervals. LB and UB are the lower bound and upper bound of the solution interval, respectively. The blue solid circles represent the extreme points in the solution interval, while the blue hollow circles represent the extreme points outside of the solution interval.

According to the Fermat's principle, the interval that contains all possible values for τ_C is

$$I_{WS} \equiv \left[\min\left(\frac{\tau_W T_{0W}}{T_{0C}}, \frac{\tau_S T_{0S}}{T_{0C}}\right), \min(\tau_{WC}, \tau_{SC})\right], \tag{41}$$

where τ_{WC} and τ_{SC} can be calculated by the method of characteristics along two edges $\overrightarrow{WC}$ and $\overrightarrow{SC}$, respectively.

In order to partition the interval I_{WS} into a few subintervals such that each subinterval contains exactly one solution, we can locate the extreme points of H as a function of τ_C and use the extreme points as the partitioning points. We can determine the extreme points by calculating the critical points through

$$\frac{\partial H}{\partial \tau_C} = \frac{\partial H}{\partial P_1}\frac{\partial P_1}{\partial \tau_C} + \frac{\partial H}{\partial Q_1}\frac{\partial Q_1}{\partial \tau_C} = 0, \tag{42}$$

which is an equation of the angle θ after algebraic manipulation, that is,

$$F(\theta) \equiv \left(\sin\theta v_m(\theta) - \cos\theta\frac{\partial v_m}{\partial \theta}\right)L_1 + \left(\cos\theta v_m(\theta) + \sin\theta\frac{\partial v_m}{\partial \theta}\right)L_2 = 0, \tag{43}$$

with

$$\begin{aligned} L_1 &= T_{0x} + \frac{T_0}{h}, \\ L_2 &= T_{0y} + \frac{T_0}{h}. \end{aligned} \tag{44}$$

From the solutions of Equation 43, denoted as $\theta_i,(i = 1,2,3,...)$, the extreme points of H as a function of τ_C can be computed by

$$\tau_C^i = \frac{\sin\theta_i T_0 \tau_S - \cos\theta_i T_0 \tau_W}{\sin\theta_i T_{0y} h + \sin\theta_i T_0 - \cos\theta_i T_{0x} h - \cos\theta_i T_0}, \quad (i = 1, 2, 3, ...). \tag{45}$$

The solutions of $F(\theta)$ can be precomputed and saved for repeated use during the Gauss-Seidel iterations. In the local solver, τ_C^i can be calculated using formula (45) to partition the interval I_{WS} into few subintervals. And then, the false position method is applied to find the solution in each subinterval. Hence, all solutions in the interval can be found.

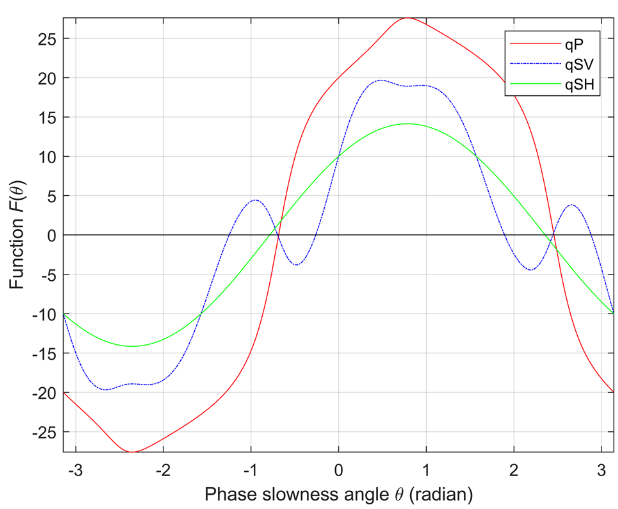

Figure 6. Curves of the critical point function $F(\theta)$ for the three wave modes in the homogeneous anisotropic model.

3.7. Solving the Discretized Equation 26

Similarly, at grid point C, the discretized Equation 26 needs to be solved for τ_C in all the four triangles. We also take ΔCWS as an example to demonstrate the procedures.

According to the Fermat's principle, the interval that contains all possible values for τ_C is

$$I_{WS} \equiv [\min(T_{0W} - T_{0C} + \tau_W, T_{0S} - T_{0C} + \tau_S), \min(\tau_{WC}, \tau_{SC})]. \tag{46}$$

The interval I_{WS} is also partitioned into few subintervals such that each each subinterval contains exactly one solution. The partitioning points are also the extreme points of H as a function of τ_C, and they can be determined by calculating the critical points through

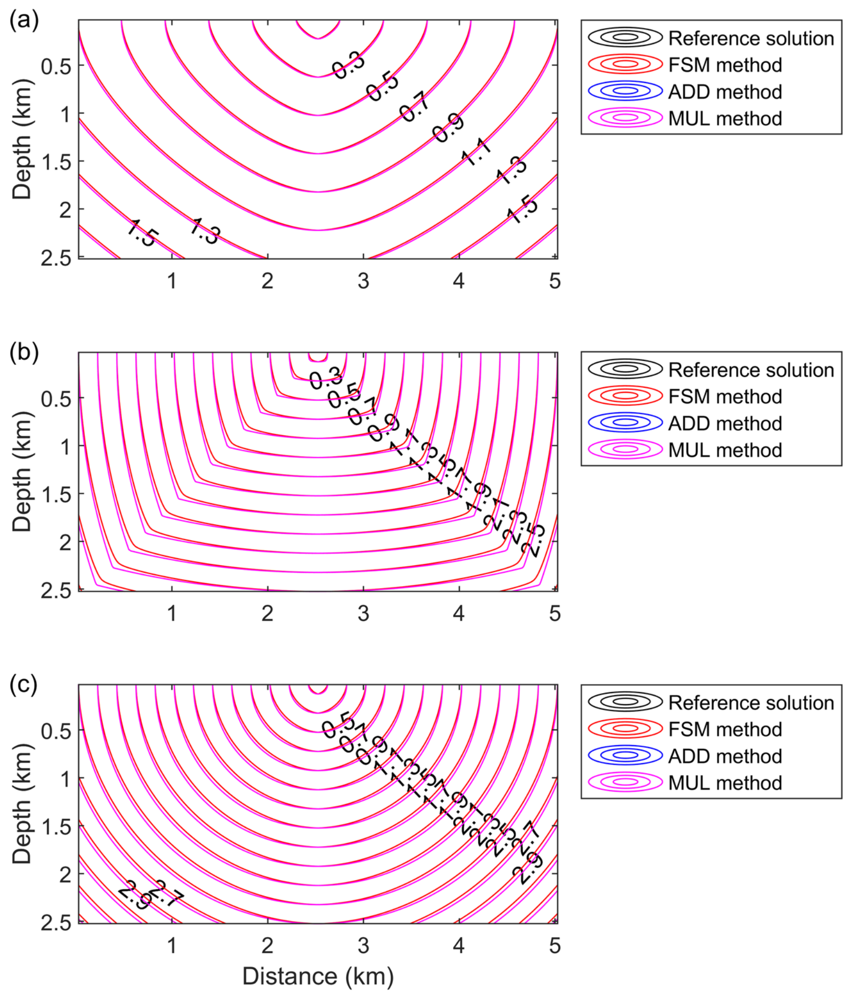

Figure 7. Traveltime comparison for the three wave modes between the reference and numerical solutions in the homogeneous anisotropic model with $\theta_0 = 0°$. Black contour line stands for the reference solution; red contour line stands for the numerical solution calculated by the FSM method; blue and magenta contour lines represent the numerical solutions calculated by the additively and multiplicatively factored FSM methods, respectively. The traveltimes are in seconds.

$$\frac{\partial H}{\partial \tau_C} = \frac{\partial H}{\partial P_2}\frac{\partial P_2}{\partial \tau_C} + \frac{\partial H}{\partial Q_2}\frac{\partial Q_2}{\partial \tau_C} = 0, \tag{47}$$

which is also an equation of the angle θ after algebraic manipulation, that is,

$$F(\theta) \equiv \left(\sin\theta v_m(\theta) - \cos\theta\frac{\partial v_m}{\partial \theta} + \cos\theta v_m(\theta) + \sin\theta\frac{\partial v_m}{\partial \theta}\right)\frac{1}{h} = 0. \tag{48}$$

Similarly, from the solutions of Equation 48, denoted as θ_i,$(i = 1,2,3,\ldots)$, we can compute the extreme points of H as a function of τ_C by

$$\tau_C^i = \frac{\cos\theta_i T_{0x} h - \sin\theta_i T_{0y} h - \cos\theta_i \tau_W + \sin\theta_i \tau_S}{\sin\theta_i - \cos\theta_i}, \quad (i = 1,\ 2,\ 3,\ \ldots\ ). \tag{49}$$

The solutions of $F(\theta)$ can be precomputed and saved for repeated use during the Gauss-Seidel iterations. In the local solver, these critical points, associated with each grid point, can be used to partition the interval I_{WS}

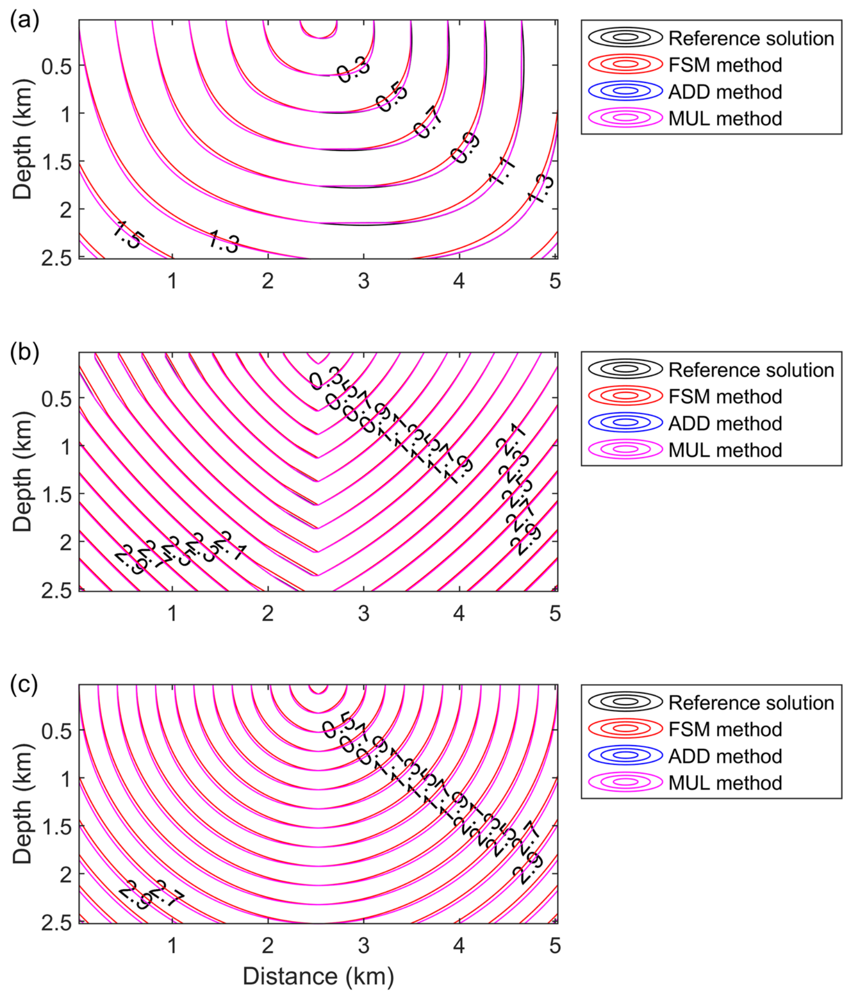

Figure 8. Traveltime comparison for the three wave modes between the reference and numerical solutions in the homogeneous anisotropic model with $\theta_0 = 45°$. Black contour line stands for the reference solution; red contour line stands for the numerical solution calculated by the FSM method; blue and magenta contour lines represent the numerical solutions calculated by the additively and multiplicatively factored FSM methods, respectively. The traveltimes are in seconds.

into few subintervals. After that, we can use the false position method to find the solution in each subinterval. Hence, all solutions in the interval can be found.

3.8. Group Velocity U_m Along Ray Direction

When calculating T_0, τ_{WC} and τ_{SC}, the group velocity U_m along a given ray direction must be determined. For example, U_m along edges is used in the local solver for a given grid point C. However, the group velocity is a function of the phase slowness direction but not a function of the ray direction. If the phase slowness direction for a given ray direction can be determined, then the group velocity along the ray direction can be computed. Previous works (Vavrycuk, 2006, 2008; Zhang & Zhou, 2018) have investigated how to calculate the slowness vector for a given ray direction.

If the phase slowness direction $\mathbf{n} = (\sin\theta, \cos\theta)$ and the phase velocity v_m are given, the slowness vector $\mathbf{p_m}$ can be written as

$$\mathbf{p_m} = \frac{\mathbf{n}}{v_m}, \quad (m = 1, 2, 3). \tag{50}$$

According to Cerveny (2001), the phase slowness vector $\mathbf{p_m}$ and the group velocity vector $\mathbf{U_m}$ should satisfy the following equation:

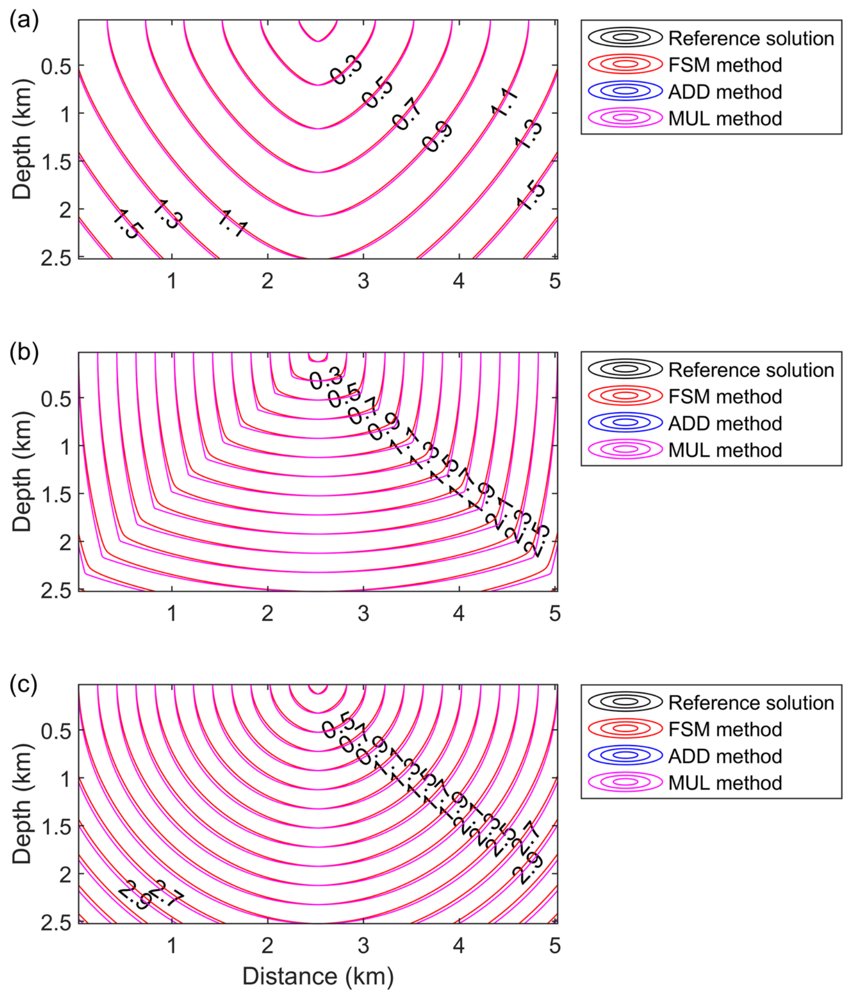

Figure 9. Traveltime comparison for the three wave modes between the reference and numerical solutions in the homogeneous anisotropic model with $\theta_0 = 90°$. Black contour line stands for the reference solution; red contour line stands for the numerical solution calculated by the FSM method; blue and magenta contour lines represent the numerical solutions calculated by the additively and multiplicatively factored FSM methods, respectively. The traveltimes are in seconds.

$$\mathbf{p_m} \cdot \mathbf{U_m} = 1. \tag{51}$$

The phase slowness direction $\mathbf{n}$ and the ray direction $\mathbf{N}$ are given as

$$\mathbf{n} = \frac{\mathbf{p_m}}{|\mathbf{p_m}|}, \quad \mathbf{N} = \frac{\mathbf{U_m}}{|\mathbf{U_m}|}. \tag{52}$$

By dividing Equation 51 with $|\mathbf{p_m}||\mathbf{U_m}|$, one can derive the following equation:

$$\mathbf{n} \cdot \mathbf{N} - \frac{v_m}{U_m} = 0. \tag{53}$$

For a given ray direction, denoted as $\mathbf{N} = (N_1, N_2)$, Equation 53 provides a way to calculate the phase slowness angle θ, as well as the phase velocity v_m and the group velocity U_m, that is, by solving the following equation:

$$G(\theta) \equiv N_1 \sin\theta + N_2 \cos\theta - \frac{v_m(\theta)}{U_m(\theta)} = 0. \tag{54}$$

Table 1
Accuracy of the First-Order FSM Method in the Homogeneous Anisotropic Model

Mesh	Iteration	L_1 error	Convergence order	Time cost (s)
qP wave mode				
101×51	1	0.0138	-	0.7
201×101	1	0.0082	0.7510	1.0
401×201	1	0.0047	0.8030	4.0
801×401	1	0.0027	0.8090	20.0
qSV wave mode				
101×51	1	0.0272	-	1.0
201×101	1	0.0153	0.8301	2.0
401×201	1	0.0084	0.8651	8.0
801×401	1	0.0046	0.8789	29.0
qSH wave mode				
101×51	1	0.0369	-	1.0
201×101	1	0.0221	0.7396	1.0
401×201	1	0.0129	0.7767	6.0
801×401	1	0.0074	0.8111	25.0

From Equation 54, we can see that the only unknown is θ. If the phase slowness angle θ is computed, then group velocity U_m and the phase velocity v_m along the ray direction $\mathbf{N}$ can be calculated.

Equation 54 can be presolved for θ, as well asfor v_m and U_m, along a set of ray directions. For example, on ΔCWS, this equation can be presolved for the two ray directions along two edges $\overrightarrow{WC}$ and $\overrightarrow{SC}$, respectively, and hence, the group velocity along these two directions can be saved for repeated use during the Gauss-Seideliterations.

3.9. Discussion of the Methods

The proposed method is developed in the framework of the FSM. Therefore, it has all the desired properties of the FSM, such as consistency, monotonicity, and convergence (Luo & Zhao, 2016; Qian et al., 2007; Zhao, 2005). The scheme is consistent with the first-order finite difference approximations; that is, the discretized equation will converge to the original equation as the mesh size approaches 0. The causality condition implies that the scheme is monotone; that is, at each grid point C, the numerical Hamiltonian H is nondecreasing with respect to the solution at C and nonincreasing with respect to the solutions at neighbor points. The consistency and monotonicity assure the stability of the scheme such that the numerical solution will converge to the viscosity solution (Barles & Souganidis, 1991; Luo & Zhao, 2016; Qian et al., 2007; Zhao, 2005), which corresponds to the first-arrival traveltime (Lions, 1982).

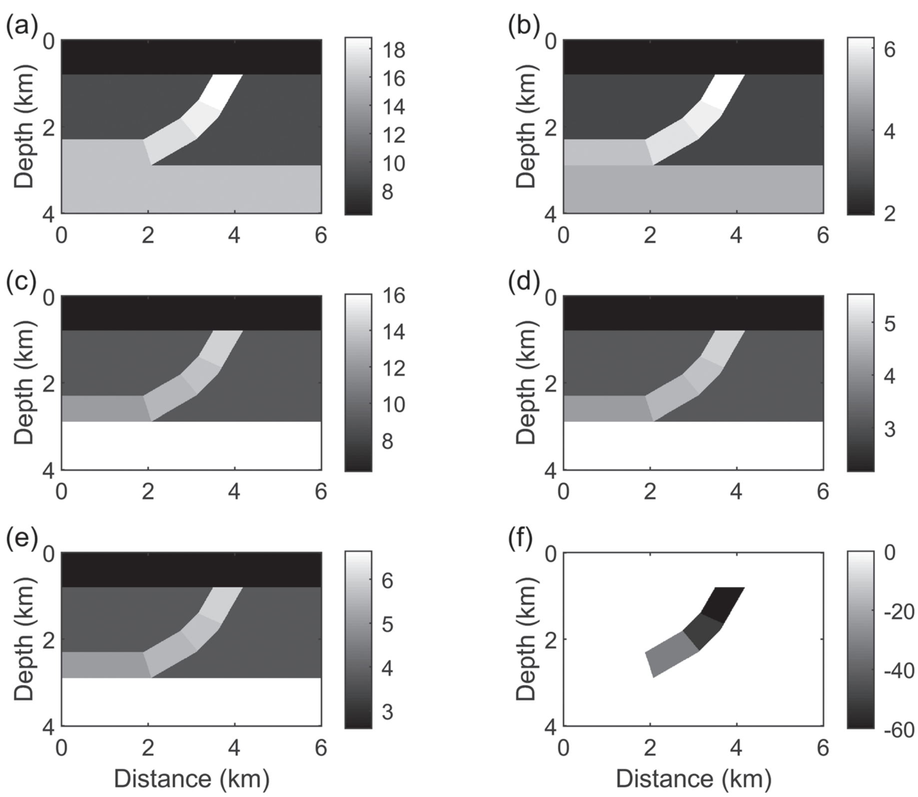

Figure 10. Anisotropic parameters of the overthrust TTI model. (a) a_{11} model, (b) a_{13} model, (c) a_{33} model, (d) a_{44} model, (e) a_{66} model, (f) θ_0 model. The scale of shades of grey is in km^2/s^2 in (a–e) and in degrees in (f).

Table 2
Accuracy of the First-Order FSM Method in the Overthrust TTI Model

Mesh	Iteration	L_1 error	Convergence order	Time cost (s)
qP wave mode				
76×51	1	0.0181	-	1.0
151×101	2	0.0101	0.8416	2.0
301×201	2	0.0061	0.7275	10.0
qSV wave mode				
76×51	1	0.0298	-	0.8
151×101	2	0.0173	0.7845	2.0
301×201	2	0.0106	0.7067	9.0
qSH wave mode				
76×51	1	0.0283	-	1.0
151×101	2	0.0161	0.8137	2.0
301×201	2	0.0099	0.7016	10.0

Similarly, as in the usual FSM, the number of iterations depends on the problems and the desired accuracy requirement. However, for a given problem with a prescribed accuracy requirement, it is independent of the mesh size as the mesh size approaches 0 (Luo & Zhao, 2016; Qian et al., 2007; Zhao, 2005).

In the local solver for solving the highly nonlinear equations to compute all possible updates at each grid point, necessary ingredients can be predetermined prior to the Gauss-Seidel iterations. That is, Equations 39, 43, 48, and 54 can be presolved with any appropriate root-finding methods, and their solutions can be saved for repeated use during the Gauss-Seidel iterations. Moreover, their solutions can be computed efficiently in parallel.

4. Numerical Examples

We present several numerical experiments to demonstrate the efficiency and accuracy of the developed methods. In the numerical implementations, we denote one iteration as four sweeps over all grid points. Numerical errors at all grid points in L_1 norm are recorded. The stopping criterion is 10^{-9}. Wherever applicable, the solutions computed by the shortest path method (SPM) on densely sampled meshes are used as the reference solutions (Huang et al., 2014; Zhou & Greenhalgh, 2006).

4.1. Homogeneous Anisotropic Model

We first use a homogeneous anisotropic model to test the effectiveness and feasibility of the proposed methods, along with demonstration of the necessary ingredients in the methods. The moduli parameters are $a_{11} = 5.2$, $a_{13} = 0.93$, $a_{33} = 4.0$, $a_{44} = 1.0$, and $a_{66} = 1.0$ km^2/s^2, and the inclination angle θ_0 is set to 0° (VTI), 45° (TTI), or 90° (HTI). The computational domain is a 5×2.5-km rectangular domain, with a point source located at $x = 2.5$ km and $y = 0$ km.

For computing the group velocity along a given ray direction, Equation 54, that is, $G(\theta) = 0$, needs to be solved. Figure 3 shows an example of the function $G(\theta)$ with $\theta_0 = 0^o$ for the three wave modes. From Figure 3, one can see that at least one root of $G(\theta)$ exists for each of the three wave modes. If more than one root exist, for example, in the case of triplication for the qSV wave (Vavrycuk, 2003a, 2003b, 2006), the one corresponding to the minimal group velocity is chosen. Figure 4 shows an example of the triplication for the qSV wave.

Table 3
Accuracy of the First-Order Additively Factored FSM Method in the Overthrust TTI Model

Mesh	Iteration	L_1 error	Convergence order	Time cost (s)
qP wave mode				
76×51	1	0.0058	-	1.0
151×101	1	0.0030	0.9511	2.0
301×201	2	0.0015	1.0000	11.0
qSV wave mode				
76×51	1	0.0103	-	2.0
151×101	2	0.0053	0.9586	5.0
301×201	2	0.0026	1.0275	25.0
qSH wave mode				
76×51	1	0.0093	-	2.0
151×101	2	0.0051	0.8667	8.0
301×201	2	0.0025	1.0286	23.0

For solving the discretized equation on a triangle at a given grid point, the roots of $F(\theta)$ are used to partition the solution interval into subintervals (see Figure 5). Figure 6 shows an example of the function $F(\theta)$ that has about two to six roots for the three wave modes. These roots correspond to the extreme points of H in the solution interval.

Traveltime tables of the qP, qSV, and qSH waves computed by the proposed methods are compared with the reference solutions in Figures 7–9. The number of iterations, L_1-norm errors, CPU times, and convergence orders are listed in Table 1. We observe the expected order of convergence $O(h\log(h))$ that is normal for the FSM. For the two factored methods, the machine error is dominant. For example, with $\theta_0 = 0^o$: for the qP wave, the maximal relative error of the original method is 0.14, and the maximal relative errors of the two factored methods are close to 2.75×10^{-5}; for the qSV wave, the maximal relative error of the original method is 0.33, and the maximal relative errors of the two factored methods are close to $8.5{\times}10^{-6}$; for the qSH wave, the maximal relative error of the original method is 0.21, and the maximal relative errors of the two factored methods are close to $1.7{\times}10^{-5}$.

Table 4
Accuracy of the First-Order Multiplicatively Factored FSM Method in the Overthrust TTI Model

qP wave mode				
Mesh	Iteration	L_1 error	Convergence order	Time cost (s)
76×51	1	0.0034	-	0.8
151×101	1	0.0014	1.2801	3.0
301×201	2	5.6251e-04	1.3155	11.0
qSV wave mode				
Mesh	Iteration	L_1 error	Convergence order	Time cost (s)
76×51	1	0.0045	-	1.0
151×101	2	0.0020	1.1699	3.0
301×201	2	7.5947e-04	1.3969	13.0
qSH wave mode				
Mesh	Iteration	L_1 error	Convergence order	Time cost (s)
76×51	1	0.0054	-	1.0
151×101	2	0.0022	1.2955	4.0
301×201	2	9.6072e-04	1.1953	15.0

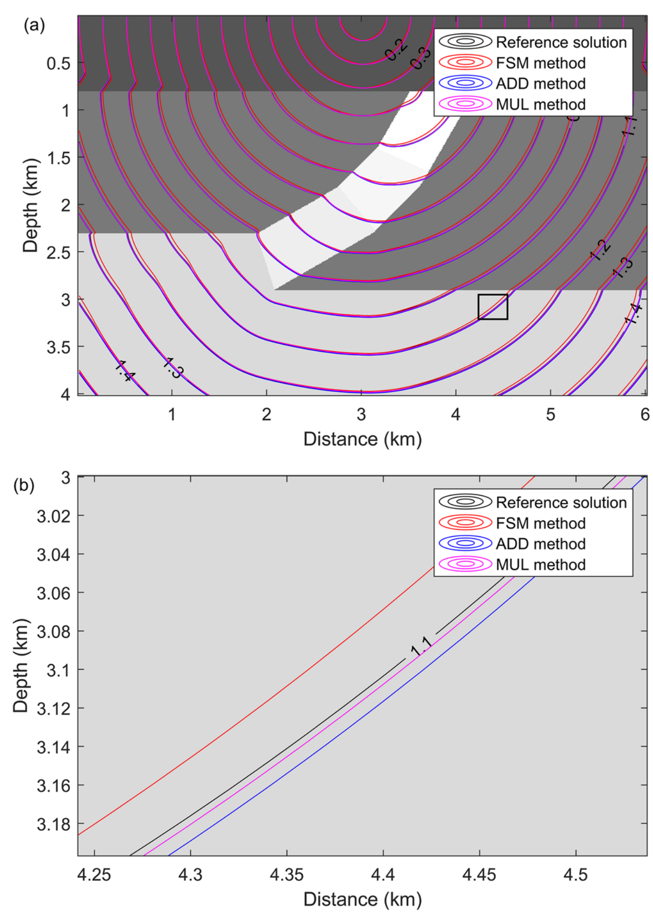

Figure 11. Comparison of the qP wave traveltimes (in sec) between the reference and numerical solutions in the overthrust TTI model. (a) Black contour line stands for the reference solution, red contour line stands for the numerical solution calculated by the FSM method, and blue and magenta contour lines represent the numerical solutions generated by the additively and multiplicatively factored FSM methods, respectively. (b) Zoom-in map of the square area as shown in (a), from which we can see that traveltimes solved by the factored methods have better accuracy.

10.1029/2019JB018868

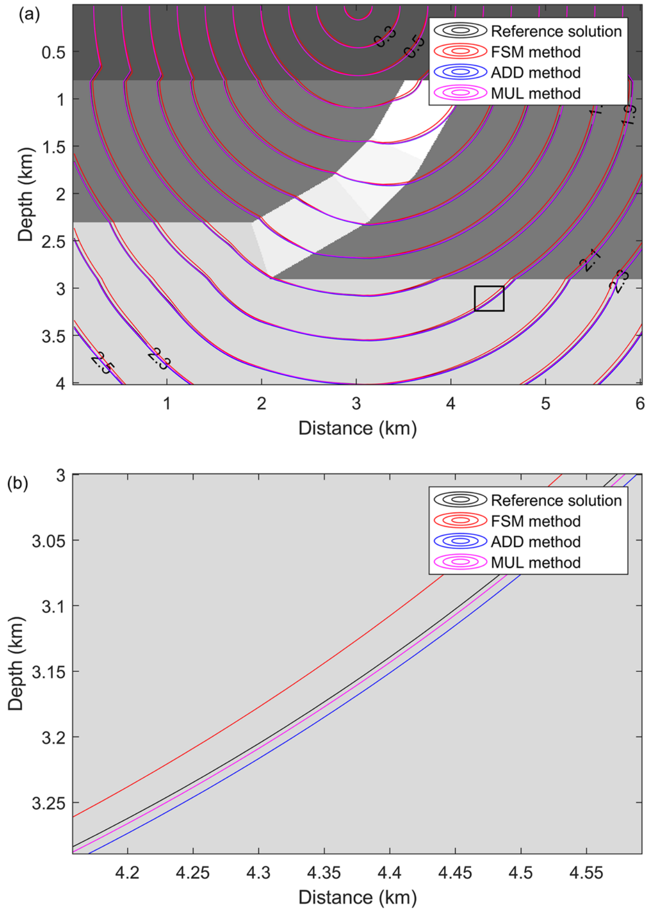

Figure 12. Comparison of the qSV wave traveltimes (in sec) between the reference and numerical solutions in the overthrust TTI model. (a) Black contour line stands for the reference solution, red contour line stands for the numerical solution calculated by the FSM method, and blue and magenta contour lines represent the numerical solutions generated by the additively and multiplicatively factored FSM methods, respectively. (b) Zoom-in map of the square area as shown in (a), from which we can see that traveltimes solved by the factored methods have better accuracy.

4.2. Overthrust TTI Model

We further test the proposed methods on the overthrust TTI model, with the model parameters shown in Figure 10. The computational domain is a 6×4-km rectangular domain with a point source located at $x = 3$ km and $y = 0$ km. The reference solution is computed by the irregular grid shortest path method (SPM) (Huang et al., 2014; Zhou & Greenhalgh, 2006) on a 601×401 mesh, with five secondary nodes added to each cell boundary in the computation. The number of iterations, L_1-norm errors, convergence orders, and CPU times are listed in Tables 2–4, where we observe a clean first-order convergence for the two factored methods. The numerical plots are presented in Figures 11–13, where we can see that the solutions match very well and the solutions computed by the two factored methods have better resolutions than those computed by the original FSM.

5. Conclusions

We present an efficient FSM for calculating first-arrival traveltimes of the three wave modes (qP, qSV, and qSH) in 2D heterogeneous, transversely isotropic media with arbitrary dipping symmetry axes. No weak anisotropy approximation is assumed, and no simplification is made to the phase and group velocities. The proposed methods enjoy all the appealing features as in the fast sweeping method for the isotropic eikonal equation (Zhao, 2005), that is, consistency, monotonicity, and convergence.

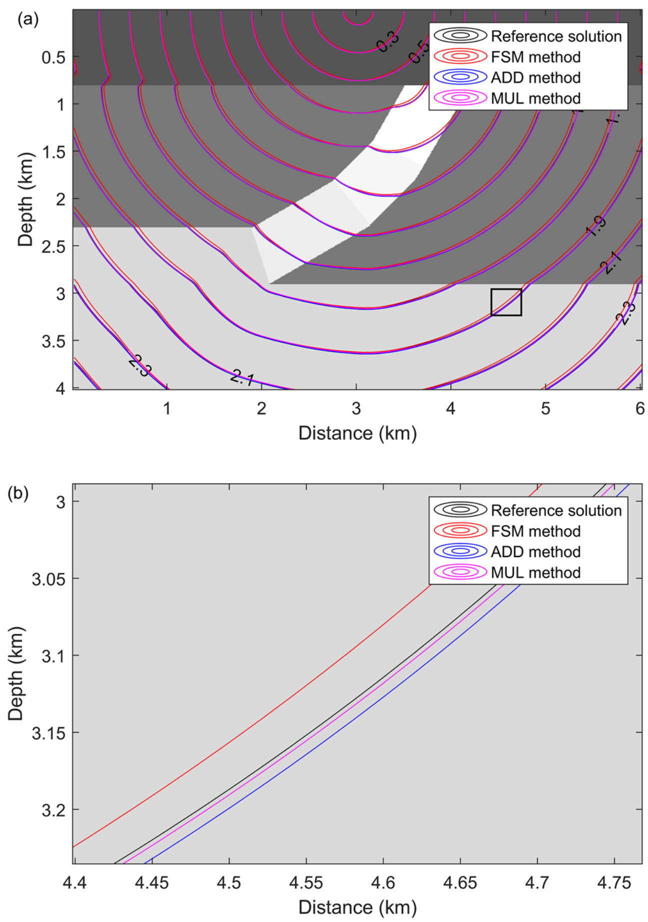

Figure 13. Comparison of the qSH wave traveltimes (in sec) between the reference and numerical solutions in the overthrust TTI model. (a) Black contour line stands for the reference solution, red contour line stands for the numerical solution calculated by the FSM method, and blue and magenta contour lines represent the numerical solutions generated by the additively and multiplicatively factored FSM methods, respectively. (b) Zoom-in map of the square area as shown in (a), from which we can see that traveltimes solved by the factored methods have better accuracy.

For problems with a point-source condition, a factorization approach is applied to resolve the source singularities such that clear first-order convergence is obtained. Numerical experiments, including a homogeneous model, a three-layered model (supporting information), and the overthrust TTI model, verify the effectiveness of the proposed methods.

Extension of the proposed methods to 3D anisotropic eikonal equation in TTI media is underway. The formulations of the methods are similar as those in 2D cases. The main difference is in Equations 39, 43, and 48 for precomputing the partitioning points and Equation 54 for computing the group velocity along a given ray direction. For 3D cases, these equations will depend on two unknown angles (just like the spherical coordinate system in 3D versus the polar coordinate system in 2D), which is more challenging than 2D cases where these equations depend on one unknown angle. Solving a nonlinear equation of two unknowns is nontrivial. An extra condition/equation is required, which can be provided through the relation among the slowness vector, the ray vector, and the symmetric axis. The resulting system of two equations will be solved to determine the two unknown angles, and the solutions can be saved and repeated used to compute the partitioning points in the Gauss-Seidel iterations, similarly as in 2D cases. We will report the results once the work is completed.

Acknowledgments
This research is jointly supported by the National Natural Science Foundation of China (41504095 and 41674077) and the China Scholarship Council. Luo was partially supported by NSF DMS (1418908 and 1719907). Model files in numerical examples can be downloaded from https://zenodo.org/record/3678494#.Xk_rj2gzY2x.

References

Alkhalifah, T., & Fomel, S. (2001). Implementing the fast marching eikonal solver: Spherical versus Cartesian coordinates. *Geophysical Prospecting*, *49*(2), 165–178.

Barles, G., & Souganidis, P. E. (1991). Convergence of approximation schemes for fully nonlinear second order equations. *Asymptotic Analysis*, *4*(3), 271–283.

Berryman, J. G. (1979). Long-wave elastic anisotropy in transversely isotropic media. *Geophysics*, *44*(5), 896–917.

Bouteiller, P. L., Benjemaa, M., Mtivier, L., & Virieux, J. (2018). An accurate discontinuous Galerkin method for solving point-source eikonal equation in 2D heterogeneous anisotropic media. *Geophysical Journal International*, *212*(3), 1498–1522.

Cao, S., & Greenhalgh, S. (1993). Calculation of the seismic first-break time field and its ray path distribution using a minimum traveltime tree algorithm. *Geophysical Journal International*, *114*(3), 593–600.

Cerveny, V. (1972). Seismic rays and ray intensities in inhomogeneous anisotropic media. *Geophysical Journal International*, *29*(1), 1–13.

Cerveny, V. (2001). *Seismic ray theory*. Cambridge: Cambridge University Press.

Cristiani, E. (2009). A fast marching method for Hamilton-Jacobi equations modeling monotone front propagations. *Journal of Scientific Computing*, *39*(4), 189–205.

Daley, P. F., & Hron, F. (1977). Reflection and transmission coefficients for transversely isotropic media. *Bulletin of the Seismological Society of America*, *67*(3), 661–675.

Dellinger, J., & Symes, W. (1997). Anisotropic finite-difference traveltimes using a Hamilton-Jacobi solver. SEG Technical Program Expanded Abstracts 1786–1789.

Eaton, D. W. S. (1993). Finite difference traveltime calculation for anisotropic media. *Geophysical Journal of the Royal Astronomical Society*, *114*(2), 273–280.

Fomel, S., Luo, S., & Zhao, H. (2009). Fast sweeping method for the factored eikonal equation. *Journal of Computational Physics*, *228*(17), 6440–6455.

Gray, S. H., & May, W. P. (1994). Kirchhoff migration using eikonal equation traveltimes. *Geophysics*, *59*(5), 810–817.

Han, S., Zhang, W., & Zhang, J. (2017). Calculating qP-wave traveltimes in 2-D TTI media by high-order fast sweeping methods with a numerical quartic equation solver. *Geophysical Journal International*, *210*(3), 1560–1569.

Hole, J. A., & Zelt, B. C. (1995). 3-D finite-difference reflection traveltimes. *Geophysical Journal International*, *121*(2), 427–434.

Huang, J., & Bellefleur, G. (2012). Joint transmission and reflection traveltime tomography using the fast sweeping method and the adjoint-state technique. *Geophysical Journal International*, *188*(2), 570–582.

Huang, G., Zhou, B., Li, H., Zhang, H., & Li, Z. (2014). 2D seismic reflection tomography in strongly anisotropic media. *Journal of Geophysics and Engineering*, *11*(6), 1–8.

Kim, S. (2002). 3D eikonal solvers, part I: First-arrival traveltimes. *Geophysics*, *67*(4), 1225–1231.

Kim, S., & Cook, R. (1999). 3-D traveltime computation using second-order ENO scheme. *Geophysics*, *64*(6), 1867–1876.

Lan, H., Chen, J., & Zhang, Z. (2014). A fast sweeping scheme for calculating P wave first-arrival travel times in transversely isotropic media with an irregular surface. *Pure and Applied Geophysics*, *171*(9), 2199–2208.

Lecomte, I. (1993). Finite difference calculation of first traveltimes in anisotropic media. *Geophysical Journal International*, *113*(2), 318–342.

Lions, P. L. (1982). *Generalized solutions of Hamilton-Jacobi equations*. Boston: Pitman Advanced Pub. Program.

Lou, M. (2006). Traveltime calculation in 3D TTI media by the fast-marching method. Expanded Abstracts in EAGE Workshop 34–39.

Luo, S., & Qian, J. (2011). Factored singularities and high-order Lax-Friedrichs sweeping schemes for point-source traveltimes and amplitudes. *Journal of Computational Physics*, *230*(12), 4742–4755.

Luo, S., & Qian, J. (2012). Fast sweeping methods for factored anisotropic eikonal equations: Multiplicative and additive factors. *Journal of Scientific Computing*, *52*(2), 360–382.

Luo, S., Qian, J., & Zhao, H. (2012). Higher-order schemes for 3D first-arrival traveltimes and amplitudes. *Geophysics*, *77*(2), T47–T56.

Luo, S., & Zhao, H. (2016). Convergence analysis of the fast sweeping method for static convex Hamilton-Jacobi equations. *Research in the Mathematical Sciences*, *3*(1), 35–62.

Noble, M., Gesret, A., & Belayouni, N. (2014). Accurate 3-D finite difference computation of traveltimes in strongly heterogeneous media. *Geophysical Journal International*, *199*(3), 1572–1585.

Perez, M., & Bancroft, J. C. (2001). Finite-difference anisotropic traveltimes and raypaths. *CREWES Research Report*, *13*, 445–461.

Pica, A. (1997). Fast and accurate finite-difference solutions of the 3D eikonal equation parametrized in celerity. SEG Technical Program Expanded Abstracts 1774–1777.

Podvin, P., & Lecomte, I. (1991). Finite difference computation of traveltimes in very contrasted velocity models: A massively parallel approach and its associated tools. *Geophysical Journal of the Royal Astronomical Society*, *105*(1), 271–284.

Press, W. H., Teukolsky, S. A., Vetterling, W. T., & Flannery, B. P. (1992). *Numerical recipes in C*, pp. 353–359. Cambridge: Cambridge University Press.

Qian, J., & Symes, W. W. (2002a). Finite-difference quasi-P traveltimes for anisotropic media. *Geophysics*, *67*(1), 147–155.

Qian, J., & Symes, W. W. (2002b). An adaptive finite-difference method for traveltimes and amplitudes. *Geophysics*, *67*(1), 167–176.

Qian, J., Zhang, Y. T., & Zhao, H. K. (2007). A fast sweeping method for static convex Hamilton-Jacobi equations. *Journal of Scientific Computing*, *31*(1-2), 237–271.

Rawlinson, N., Hauser, J., & Sambridge, M. (2008). Seismic ray tracing and wavefront tracking in laterally heterogeneous media. *Advances in Geophysics*, *49*, 203–273.

Sethian, J. A., & Popovici, M. A. (1999). 3-D traveltime computation using the fast-marching method. *Geophysics*, *64*(2), 516–523.

Sethian, J. A., & Vladimirsky, A. (2003). Ordered upwind methods for static Hamilton-Jacobi equations: Theory and algorithms. *SIAM Journal on Numerical Analysis*, *41*(1), 325–363.

Shearer, P. M., & Chapman, C. H. (1988). Ray tracing in anisotropic media with a linear gradient. *Geophysical Journal International*, *94*(3), 575–580.

Stovas, A., & Alkhalifah, T. (2012). A new traveltime approximation for TI media. *Geophysics*, *77*(4), C37–C42.

Tavakoli, B. F., Ribodetti, A., Virieux, J., & Operto, S. (2015). An iterative factored eikonal solver for TTI media. SEG Technical Program Expanded Abstracts 3576–3581.

Thomsen, L. (1986). Weak elastic anisotropy. *Geophysics*, *51*(10), 1954–1966.

Treister, E., & Haber, E. (2016). A fast marching algorithm for the factored eikonal equation. *Journal of Computational Physics*, *324*(1), 210–225.

Treister, E., & Haber, E. (2017). A multigrid solver to the Helmholtz equation with a point source based on travel time and amplitude. *Numerical Linear Algebra With Applications*, *26*(1), 1–20.

Tsai, Y.-H. R., Cheng, L.-T., Osher, S., & Zhao, H.-K. (2003). Fast sweeping algorithms for a class of Hamilton-Jacobi equations. *SIAM Journal on Numerical Analysis*, *41*(2), 673–694.

Vavrycuk, V. (2003a). Generation of triplications in transversely isotropic media. *Physical Review B*, *68*(5), 054107. https://doi.org/10.1103/PhysRevB.68.054107
Vavrycuk, V. (2003b). Parabolic lines and caustics in homogeneous weakly anisotropic solids. *Geophysical Journal International*, *152*(2), 318–334. https://doi.org/10.1046/j.1365-246X.2003.01845.x
Vavrycuk, V. (2006). Calculation of the slowness vector from the ray vector in anisotropic media. *Proceedings of the Royal Society A Mathematical Physical and Engineering Sciences*, *462*(2067), 883–896. https://doi.org/10.1098/rspa.2005.1605
Vavrycuk, V. (2008). Real ray tracing in anisotropic viscoelastic media. *Geophysical Journal International*, *175*(2), 617–626. https://doi.org/10.1111/j.1365-246X.2008.03898.x
Vidale, J. (1988). Finite-difference calculation of travel times. *Bulletin of the Seismological Society of America*, *78*(6), 2062–2076.
Vidale, J. (1990). Finite-difference calculation of traveltimes in three dimensions. *Geophysics*, *55*(5), 521–526.
Vinje, V., Iversen, E., & GjoYstdal, H. (1993). Traveltime and amplitude estimation using wavefront construction. *Geophysics*, *58*(8), 1157–1166.
Waheed, U. B., & Alkhalifah, T. (2017). A fast sweeping algorithm for accurate solution of the tilted transversely isotropic eikonal equation using factorization. *Geophysics*, *82*(6), WB1–WB8.
Waheed, U. B., Yarman, C. E., & Flagg, G. (2014). An iterative fast sweeping based eikonal solver for tilted orthorhombic media. SEG Technical Program Expanded Abstracts 480–485.
Waheed, U. B., Yarman, C. E., & Flagg, G. (2015). An iterative, fast-sweeping based eikonal solver for 3D tilted anisotropic media. *Geophysics*, *80*(3), C49–C58.
Zhang, L., Rector, J. W., & Hoversten, G. M. (2005). Eikonal solver in the celerity domain. *Geophysical Journal International*, *162*(1), 1–8.
Zhang, L., & Zhou, B. (2018). Calculation of slowness vector from ray directions for qP- qSV- and qSH-wave in tilted transversely isotropic media. *Geophysics*, *83*(4), C153–C160.
Zhao, H. (2005). A fast sweeping method for eikonal equations. *Mathematics of Computation*, *74*(250), 603–628.
Zhou, B., & Greenhalgh, S. (2004). On the computation of elastic wave group velocities for a general anisotropic medium. *Journal of Geophysics and Engineering*, *1*(3), 205–215.
Zhou, B., & Greenhalgh, S. (2006). Raypath and traveltime computations for 2D transversely isotropic media with dipping symmetry axes. *Exploration Geophysics*, *37*(3), 150–159.